Understanding Pacific Ocean influence on interannual precipitation variability in the Sahel

Catherine Pomposi[1], Alessandra Giannini[2], Yochanan Kushnir[3], and Dong Eun Lee[3]

[1]Department of Earth and Environmental Sciences, Columbia University, New York, New York, USA, [2]International Research Institute for Climate and Society, Palisades, New York, USA, [3]Lamont–Doherty Earth Observatory, Palisades, New York, USA

Abstract Moisture budget decomposition is performed for the Sahel (10°–20°N and 20°W–40°E) in order to understand the processes that govern regional hydroclimate variability on interannual time scales and frame them in the context of their primary ocean driver. Results show that warm conditions in the Eastern Tropical Pacific remotely force anomalously dry conditions primarily through affecting the low-troposphere mass divergence field. This behavior is related to increased subsidence over the tropical Atlantic and into the Sahel and an anomalous westward flow of moisture from the continent, both resulting in a coherent drying pattern. Understanding the physical processes relating remote sea surface temperature anomalies to atmospheric circulation changes and the resulting complex local convergence patterns is important for advancing seasonal prediction of precipitation over West Africa.

1. Introduction

The Sahel region is defined as the narrow strip of land stretching east-west across Africa and encompassing the area between 10° and 20°N. It lies in the middle of a steep rainfall gradient where yearly rainfall accumulations have recently ranged from ~300 mm to ~800 mm [*Nicholson and Webster*, 2007], primarily as a result of the West African Monsoon (WAM). It is this seasonally reversing low-level wind pattern that delivers moisture-enhanced air from the Atlantic to the region via westerly wind flow throughout the summer months July–September (JAS). Because the WAM delivers the majority of annual precipitation to the Sahel, understanding its development and variability is of great importance both scientifically and for the region's millions of inhabitants.

Sahel precipitation exhibits considerable variability on a broad range of timescales from intraseasonal and interannual to decadal and beyond [*Nicholson*, 2000; *Lebel et al.*, 2003]. These are associated with and primarily driven by variations of sea surface temperature (SST) in the major ocean basins [*Folland et al.*, 1986; *Palmer*, 1986; *Rowell et al.*, 1995; *Ward*, 1998; *Rowell*, 2001; *Giannini et al.*, 2003; *Bader and Latif*, 2003; *Hoerling et al.*, 2006; *Hagos and Cook*, 2008; *Lu*, 2009]. The majority of studies have concluded that decadal variability in the Sahel is driven by ocean basins also displaying large variability on this timescale, i.e., the Atlantic and Indian Oceans [*Giannini et al.*, 2003; *Bader and Latif*, 2003; *Hagos and Cook*, 2008; *Lu*, 2009; *Pomposi et al.*, 2014], while faster, interannual fluctuations are fundamentally remotely forced by tropical Pacific SST variations associated with the El Niño–Southern Oscillation (ENSO) [*Folland et al.*, 1986; *Rowell et al.*, 1995; *Janicot et al.*, 1996, 1998, 2001; *Ward*, 1998; *Rowell*, 2001; *Giannini et al.*, 2003].

The major focus of this study is to explore the mechanisms governing remote ocean influence on variability of the WAM on the interannual timescale. We emphasize the role of ENSO forcing in the hydrological balance, i.e., the moisture flux convergence pattern over the Sahel and the resulting precipitation fluctuations. By decomposing the moisture budget into contributions from specific humidity advection, circulation changes that affect mass convergence, and changes in moisture transport convergence by subseasonal eddies, we can identify the primary process(es) that govern the change in net surface moisture flux (precipitation-evaporation or *P-E*) [*Seager et al.*, 2010]. The utility of such a diagnostic approach has been demonstrated for observed precipitation variability in the Southeastern U.S. [*Li et al.*, 2013], future projections of midlatitude hydroclimate [*Seager et al.*, 2010], as well as for the WAM annual cycle [*Fontaine et al.*, 2003; *Thorncroft et al.*, 2011]. More recently, we investigated the case of the 20th century "decadal shift" in Sahel rainfall [*Pomposi et al.*, 2014], and here we employ a similar approach to study the changes in mechanisms of moisture convergence on the interannual timescale, addressing the following:

1. What are the physical mechanisms that govern ocean-forced variability in the region, specifically dry conditions?
2. How do these relate to prior hypotheses regarding the dynamics of "remote" and "local" oceanic influences on monsoon variability across the tropics [see *Giannini*, 2010; *Seth et al.*, 2011] and particularly in the Sahel?

2. Data and Methods

2.1. Observations and Model

Observational precipitation data utilized are from the University of East Anglia Climatic Research Unit (CRU) TS 3.2.2 data set [*Harris et al.*, 2014]. This data set is based on rain gauge observations that are interpolated to a 0.5° latitude/longitude grid.

As in *Pomposi et al.* [2014], after validating the model simulation of the association between anomalous global SST and African precipitation, we use the output to clearly attribute causality to SST changes and discern the underlying physical mechanisms of Sahel precipitation variability. The model employed is the atmospheric component of the National Center for Atmospheric Research (NCAR) Community Earth System model version 1.2, which is referred to as CAM5 [*Neale et al.*, 2012] with T42 horizontal resolution and 30 vertical levels. CAM5 is forced by monthly varying, historical SST observations and sea ice concentration from the UK Met Office's Hadley Centre (HADISST1) [*Rayner et al.*, 2003] to produce an ensemble of 16 members, each over 150 years in length and differing only in their initial atmospheric state. The resulting Global Ocean Global Atmosphere (GOGA) runs were ensemble averaged to determine the leading modes of precipitation and SST covariability (see below). We stipulate that forcing CAM5 with global SSTs and taking the ensemble mean will minimize other effects on Sahel (and global) rainfall variability (e.g., reduce the influence of weather and other non-SST-related variability and the corresponding land-atmosphere interactions) and retain primarily the SST-forced component. For other calculations, including computing the variability of the model and budget terms, each ensemble member was operated on separately before ensemble averaging. Variables are presented as averages for the peak monsoon season, JAS, during the years 1979–2008. Selection of this time period ensures that results are characteristic of interannual fluctuations and not confounded by the large-scale decadal shift in precipitation that occurred prior to 1970.

2.2. Analysis

Maximum Covariance Analysis (MCA) [*Bretherton et al.*, 1992] is used to extract the simultaneous seasonal mean relationship between the prescribed global SST anomalies and Sahel rainfall on the interannual timescale as represented in observations and the CAM5 ensemble average output, both of which are detrended before computing the MCA. From this analysis, we determine the region of the global ocean that is best correlated with interannual changes in Sahel rainfall and regress JAS anomalies on an appropriate SST index, in this case the standardized Niño 3.4 index [*Kaplan et al.*, 1998] (measuring anomalies in the Pacific between 5°N–5°S and 170°W–120°W). Regressions are thus interpreted as amount change per standard deviation change in SST.

The mechanisms by which remote SSTs influence Sahel precipitation are studied by adopting the atmospheric moisture budget approach, which equates the net change in moisture flux at the surface (*P-E*) with the vertically integrated total moisture flux convergence. The latter is then broken down into the time mean and eddy components as outlined in *Seager and Henderson* [2013]. Represented in its discrete form from $k = 1$ to K pressure levels, the moisture budget can be written as

$$\rho_w g(\overline{P} - \overline{E}) = \sum_{k=1}^{K} -\nabla \cdot \left[\left(\overline{\boldsymbol{V_k} \, q_k} \right) + \left(\overline{\boldsymbol{V'_k} \, q'_k} \right) \overline{dp_k} \right] \qquad (1)$$

where ρ_w is the density of water, g is gravitational acceleration, P denotes precipitation, E is surface evaporation, q is specific humidity, and $\boldsymbol{V}$ is the horizontal wind vector. The summation is completed on the model's original hybrid-sigma pressure grid.

As shown in equation (1), by taking the monthly mean, the total moisture flux convergence is divided into two components, one due to convergence of moisture transport by the mean flow and another due to convergence by transient eddies (first and second terms on the right-hand side, respectively). In this equation, an overbar represents individual monthly means, and primes denote departures from monthly means.
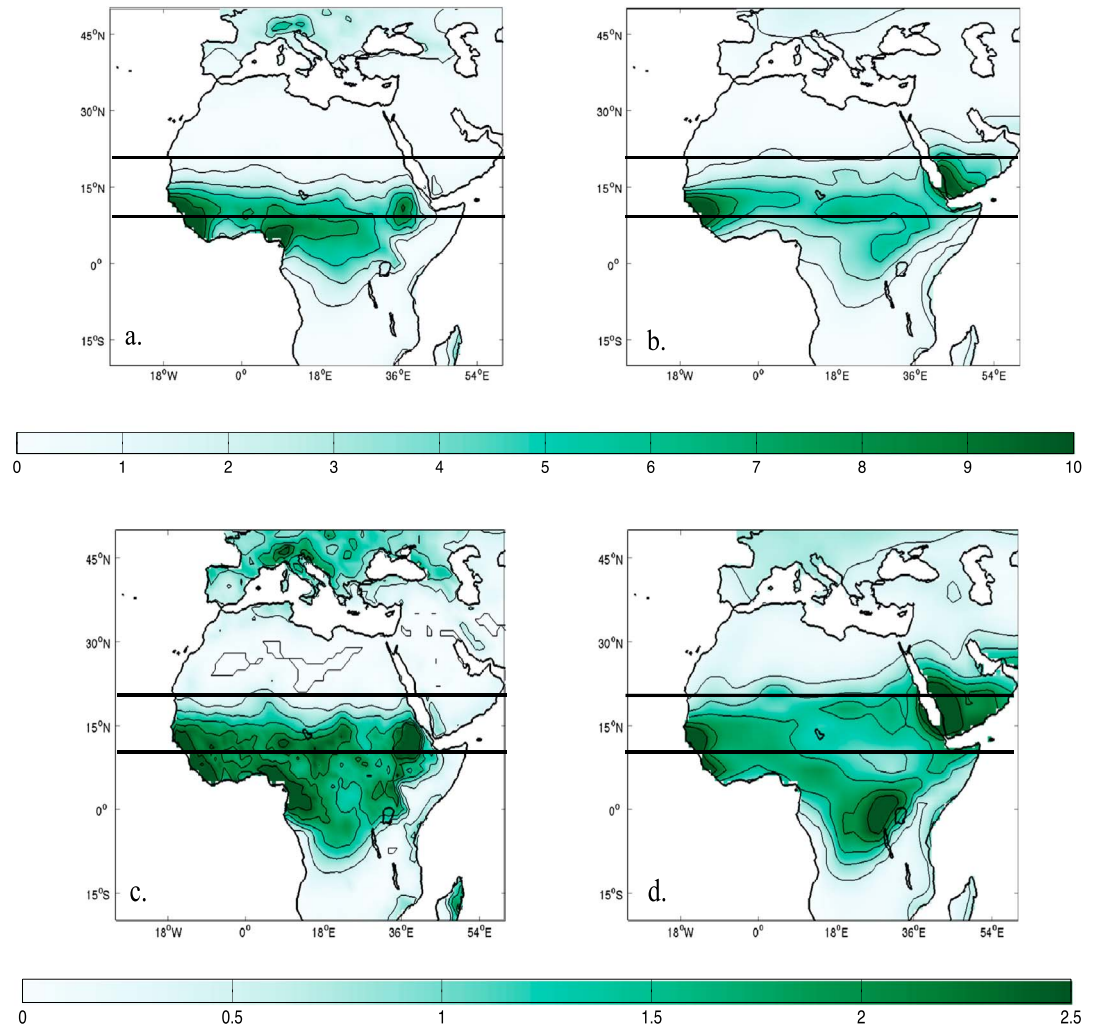
Figure 1. JAS precipitation climatology (mm/d) for (a) CRU and (b) GOGA CAM5. Contours with intervals from 2 to 10 by 2. JAS root-mean-square (RMS) anomaly (mm/d) for (c) CRU and (d) GOGA CAM5. Contours with intervals from 0.5 to 2.5 by 0.5. Sahel latitudes are outlined (10°–20°N).

The mean flow moisture convergence can then be subdivided into two components (equation (2)), one associated with mass convergence (first term on the right-hand side) and the other with advection of specific humidity (i.e., with the moisture flux convergence associated with humidity gradient even in the absence of mass convergence, second term on right-hand side):

$$\rho_w g\left(\overline{P} - \overline{E}\right) = -\left[\sum_{k=1}^{K}\left(\overline{q_k}\nabla\cdot\overline{\boldsymbol{V}_k} + \overline{\boldsymbol{V}_k}\cdot\overline{\nabla q_k}\right)\overline{dp_k} + \sum_{k=1}^{K}\nabla\cdot\left(\overline{\boldsymbol{V'}_k q'_k}\right)\overline{dp_k}\right] \tag{2}$$

JAS seasonal means are presented, derived from the monthly data used to compute budget terms in the manner just described. The moisture budget terms are computed for each ensemble member separately so we can correctly capture processes contributing to the hydroclimatic variability. Finally, these are averaged across all members to reduce variability not related to SST forcing.

3. Results

Figures 1a and 1b show the JAS precipitation climatology in observations and the CAM5 GOGA ensemble mean, respectively. Both data sets show the strong north-south precipitation gradient characteristic of the Sahel, with maximum rates in excess of 10 mm/d that decline to ~2 mm/d at the region's northern margin, as well as a local maximum in rainfall on the west coast (rates exceeding 10 mm/d) that represents the
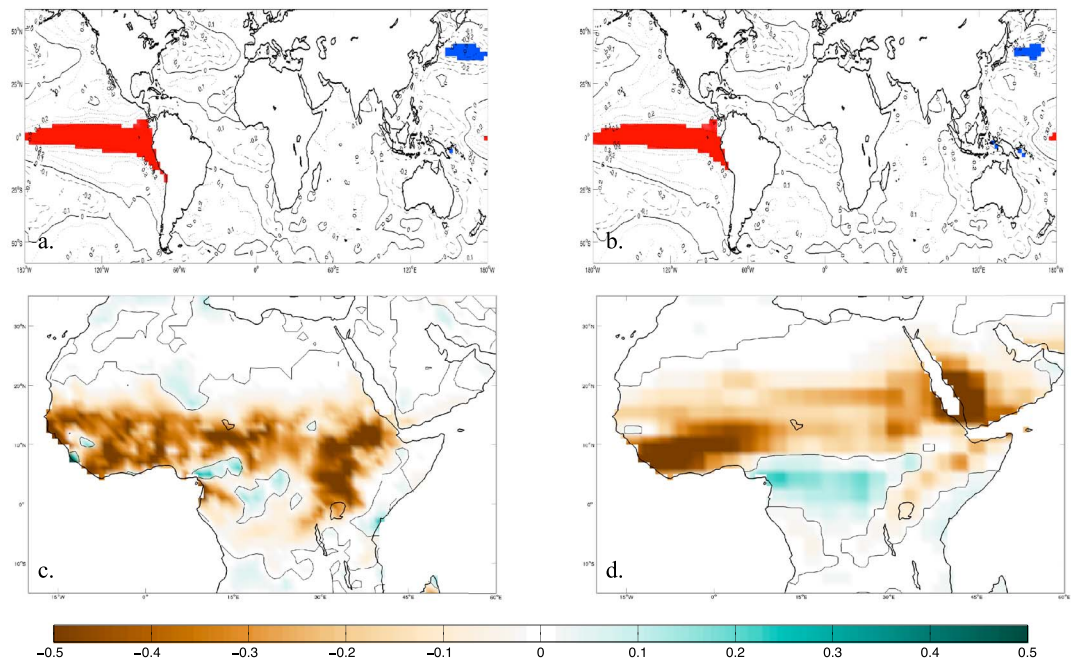
Figure 2. Regression of JAS 1979–2008 SST (°C) anomalies (contours, −0.5 to 0.5 by 0.1) on the standardized SST index derived from the MCA for (a) observations and (b) model. Shading indicates regions where the regression is significant at $\alpha = 0.05$. Regression of JAS 1979–2008 precipitation (mm/d) anomalies (colors) on the same index for (c) observations and (d) model. The zero contour is shown in black.

extension of the Atlantic Marine Intertropical Convergence Zone (ITCZ) onto land. The model underestimates the climatological precipitation rates along the Gulf of Guinea and equatorial Africa. On the other hand, the 2 mm/d precipitation contour, a rough approximation of the Sahel's northern extent, displays a slight northeastward tilt in CAM5 compared to observations. This results in a slight wet bias (Figure S1 in the supporting information) and also impacts ENSO's teleconnection to the Sahel (discussed later). The model also does not represent well the regional precipitation maximum over the Ethiopian Highlands, placing it instead over the southern Red Sea. This could be related to the relatively low resolution in the presence of complex topography as well as to the tendency of models with prescribed SSTs to rain too much over warm sea and ocean areas.

Figures 1c and 1d show, respectively, the observed and pooled model root-mean-square (RMS) precipitation variability for the core monsoon season. In the observations (Figure 1c), the temporal variability of rainfall in the region ranges from 0.5 mm/d at the Sahel's northern margin to 2.5 mm/d in the region of maximum precipitation along the coast. Variability is slightly underestimated by the model and there is less regional heterogeneity than the observations suggest. This is partly due to the model simulation being completed on a coarser horizontal grid; Stronger agreement exists when CRU is interpolated to the common ~2.8° resolution latitude/longitude grid (Figure S2). Notably, both the precipitation climatology and RMS anomaly in CAM5 exhibit substantial improvements over its predecessor CAM4, especially in the latitudinal structure of both fields which diminishes a strong northeastern bias [see *Pomposi et al.*, 2014], and precipitation characteristics across all Sahel grid boxes are realistic when compared to a number of observational data sets (Figure S1). Thus, we judge as satisfactory the model representation of overall precipitation features.

Next, we highlight the major mode of interannual covariability between SST and precipitation, providing a foundation on which to study the associated model moisture budget characteristics. Figure 2 shows the result of the MCA applied to the JAS seasonally averaged Hadley SST and African precipitation. Figures 2a and 2b show the regression of SST anomalies on the leading MCA pattern of SST for the observations and the model, respectively. ENSO is clearly indicated as the leading cause of covariation with Sahel rainfall on interannual timescales, similar in both data sets. When SST anomalies in the Eastern Tropical Pacific are warmer than normal and the Western Tropical Pacific is colder than normal (characteristic of El Niño), drought

conditions exist in sub-Saharan Africa (Figures 2c and 2d). This same ocean region exhibits significant inter-annual variability as indicated by an *F* test (not shown) and has been shown previously to influence the Sahel's high-frequency precipitation variability [e.g., *Giannini et al.*, 2003]. We also note the presence of SST anomalies in the equatorial Atlantic and positive anomalies in the Indian Ocean. Part of this SST distribution can be the result of ENSO forcing [e.g., *Alexander et al.*, 2002], but the appearance of the anomalies in the MCA pattern can also be a result of the analysis itself, which attempts to optimize the covariance between relating SST and land precipitation patterns during a limited time interval. The combination of these effects may result in ambiguity in attributing the precipitation change to a single SST source; this ambiguity will be addressed later (see also Figures S4 and S5).
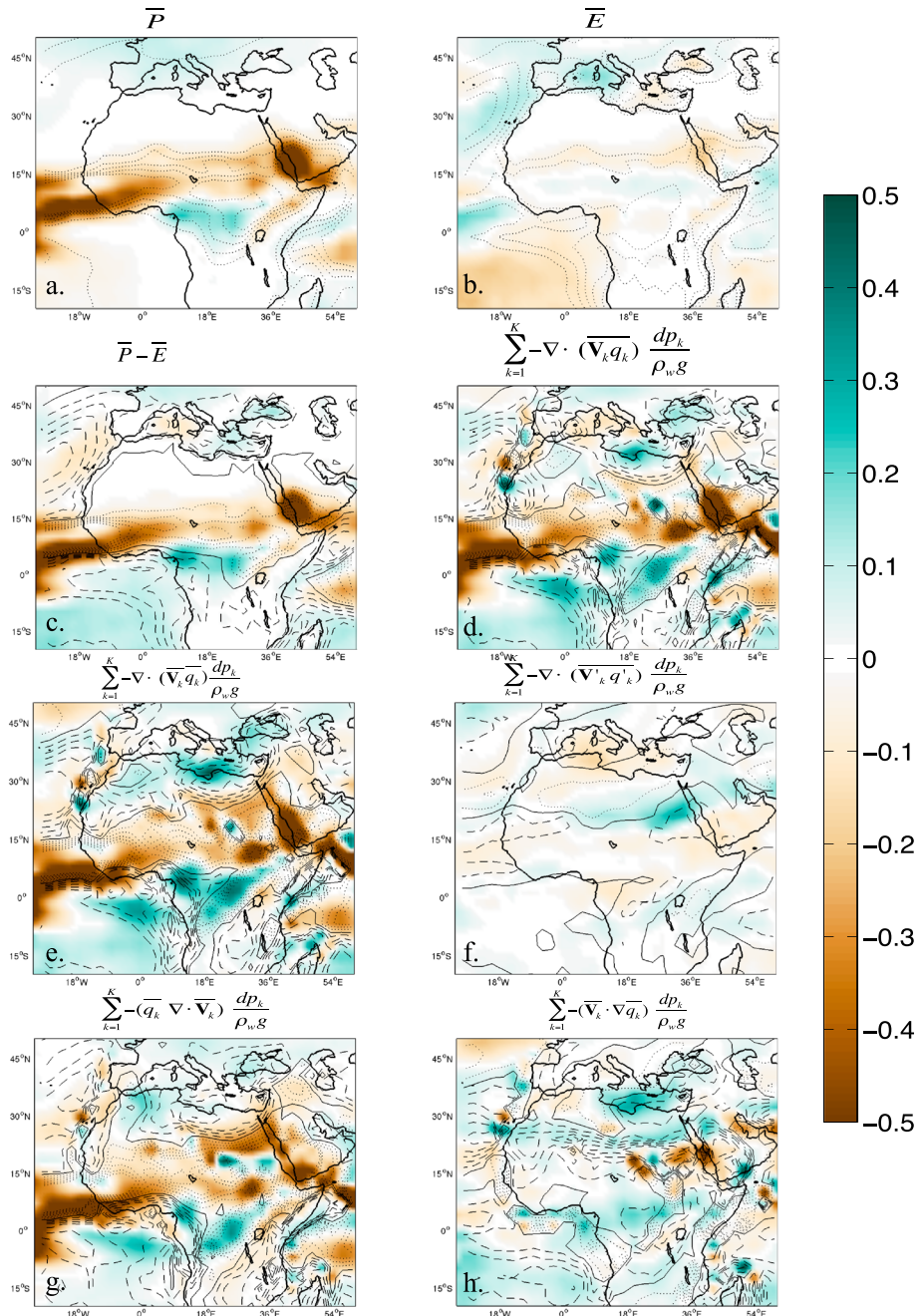
Regression of precipitation anomalies on the same MCA-derived interannual SST indices (Figures 2c and 2d) show that dry conditions in the Sahel are associated with a warm Eastern Tropical Pacific (i.e., an El Niño state), as evidenced in both the observations (Figure 2c) and CAM5 (Figure 2d). In both data sets the dry pattern extends even beyond the Sahel and more broadly throughout the WAM region to the Gulf of Guinea coast. Dry anomalies along the coast are particularly pronounced in CAM5. We find that this is due to the overly zealous response to SST anomalies in the Atlantic basin (Figure S5) compared to the observations. On the other hand, dry anomalies in the Sahel forced by ENSO are underestimated in the model. This suggests that the strength of the teleconnection is underestimated in CAM5 perhaps due to other processes that reinforce the drying in nature but are not well represented in the model (e.g., land surface feedback), or because of inherent biases in the model's simulation of ENSO's teleconnection to the Sahel. The latter includes a southward shift of the response confirmed in the climatology (not shown) and the finding that the ENSO teleconnection in the West Sahel is not statistically significant in the model ensemble mean (Figure S3). The above discussion helps to explain why Sahel precipitation does not respond as strongly to the forcing in Figure 2b as observations suggest. Nonetheless, despite these limitations, the model response to ENSO is consistent and similar to observations.

To study the mechanisms of moisture convergence driven by the leading mode of SST variability on the inter-annual timescale (i.e., ENSO), we regress the JAS moisture budget anomalies on the standardized Niño 3.4 index (Figure 3). This observational index is selected rather than the MCA-derived index in order to control for the influence of equatorial Atlantic and Indian SST anomalies previously described. Even so, we confirm that there still exists significant covariability during JAS in the Southern Equatorial Atlantic with ENSO (Figure S4). Thus, to more clearly distinguish the roles of each of the individual basins, accounting for effects of their covariations with one another, we complete a multiple linear regression with both indices and confirm the dominant role of ENSO forcing dry conditions in the Sahel (Figure S5).

In Figure 3a, negative precipitation anomalies (colors) are evident east-west across the continent between about 5°N and 20°N. Comparison with the climatology (contours) reveals that the reduction in precipitation during El Niño events influences the entire summer rain band and extends throughout West Africa to the Gulf of Guinea. Drying is pronounced here because the model responds too strongly to Atlantic forcing, particularly the cold conditions in the Southern Equatorial Atlantic (see comments above and Figure S5).

A reduction in the evaporation (Figure 3b) from the land surface occurs over a much narrower strip of land, confined to about 15°N–20°N, consistent with reduced precipitation, and hence soil moisture. The anomalous evaporation (Figure 3b) is only a fraction of its climatological value and does not follow the spatial structure of the precipitation field. Thus, the spatial pattern and magnitude of net surface moisture (*P-E*) anomalies (Figure 3c) are mostly influenced by the reductions in precipitation (Figure 3a). The largest declines in *P-E* occur roughly in the same area where the largest climatological *P-E* values are found (i.e., along the Gulf of Guinea and stretching northeastward into the continent).

The total moisture flux convergence (Figure 3d) roughly balances *P-E* as expected, showing strong divergence of moisture over the coast along the Gulf of Guinea and northward into the Sahel characterizing the region's dry phase. There are also centers of strong moisture divergence in parts of East Africa and the nearby Red Sea. Anomalous moisture flux divergence associated with El Niño dominates throughout the entire region where the climatological (contours) moisture flux converges, consistent with the precipitation changes. This anomalous moisture divergence is accomplished mostly by the mean flow moisture flux convergence (Figure 3e), which clearly dominates the magnitude of drying over divergence of moisture by transients (Figure 3f). In

Figure 3. JAS moisture budget anomalies regressed on the standardized Niño 3.4 index for (a) precipitation, (b) evaporation, (c) P-E, (d) total moisture flux convergence, (e) moisture convergence by the mean flow, (f) moisture convergence by the transient flow, (g) mass convergence, and (h) specific humidity advection. All terms have been converted to mm/d with convergence (divergence) in green (brown). Climatologic contours are shown for comparison and are from −5 to 5 by 1 mm/d with dotted (dashed) contours denoting convergence (divergence). The zero contour is shown in black.

some cases, such as around 18°N, particularly in the east, the transients work to converge moisture and offset the drying pattern.

In subdividing the moisture convergence by the mean flow into a term associated with mass convergence (Figure 3g) and another with specific humidity advection (Figure 3h), it becomes clear that mass convergence is the dominant player in the budget associated with ENSO forcing. Strong mass divergence occurs over the tropical Atlantic and throughout the Sahel during El Niño, contributing the most to the decline in net
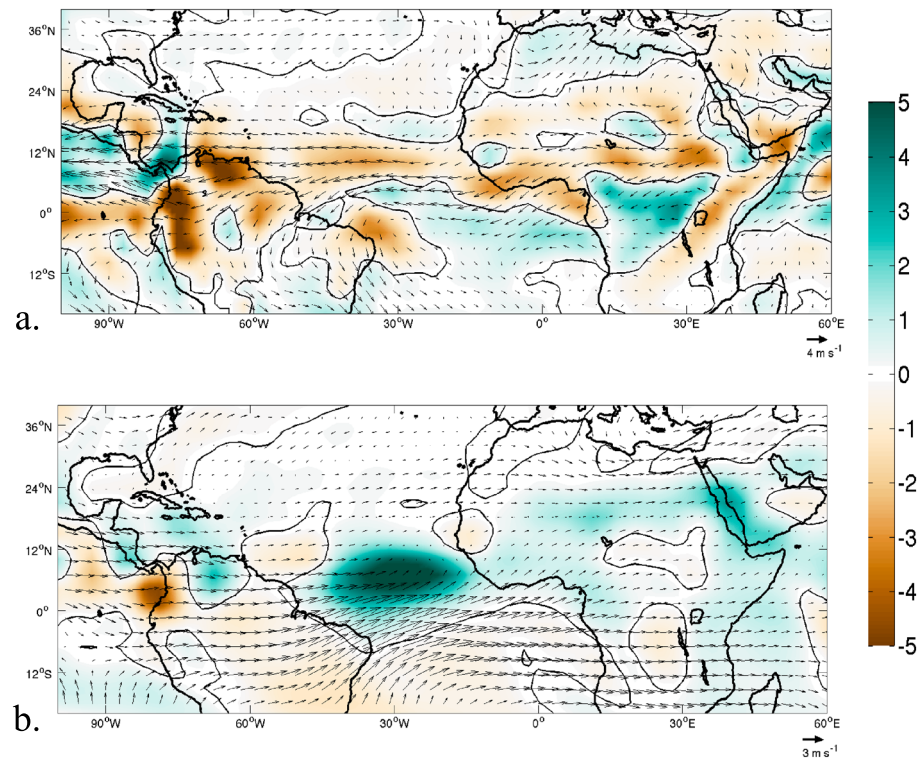
Figure 4. Regression of JAS horizontal wind (vectors) and mass convergence (colors) anomalies on standardized Niño 3.4 index for (a) 850 mb and (b) 200 mb. Green (brown) denotes convergence (divergence). Note the difference in magnitude; in Figure 4a mass convergence is scaled by 10^{-3} and in Figure 4b mass convergence is scaled by 10^{-5}. The zero contour is shown in black.

moisture flux at the surface. Specific humidity advection (Figure 3h) weakly dries the region, increasing in magnitude as one travels eastward across the Sahel, to cause stronger drying east of ~30°E. That ENSO influences the Sahel primarily through a dynamical response and associated effects on the overall atmospheric circulation in the tropics is consistent with prior studies including *Janicot et al.* [1996] and *Rowell* [2001] and is supported by the dominant role of the mass convergence term in the present study. In the model, advection of moisture wets the band bordering on the northern edge of the Sahel to partially oppose the mass convergence term. This is related to the circulation change in the presence of the climatological moisture gradient over North Africa (Figure 4).

In order to provide a clearer explanation of ENSO's control on interannual variability in the region, we consider the horizontal wind field (vectors) at two pressure levels in the lower and upper troposphere, along with the mass convergence field (colors), extending the domain to include the easternmost portion of the Pacific basin. At the 850 mb level, anomalous divergence of mass is evident throughout the region (Figure 4a), primarily due to the westward flow that develops in association with increased convergence over the warmer than normal Eastern Equatorial Pacific. Specifically, these wind anomalies can be interpreted in part as a Gill-Matsuno-type response, driven by the warm anomaly in the Eastern Tropical Pacific and subsequent atmospheric heating that occurs during El Niño (see also *Kucharski et al.* [2009]). Warming over the Eastern Tropical Pacific sets up an east-west pressure gradient that favors anomalous westward flow across Africa at low levels (Figure 4a), consistent with anticyclonic flow that stretches from the Eastern Pacific to the Atlantic basin. The anomalous winds drive moisture out of West Africa and the Sahel at this critical, moist atmospheric level whose wind characteristics are important for characterizing dry or wet years [*Grist and Nicholson*, 2001].

The anomalous flow pattern is reversed at upper levels (Figure 4b) where the flow is eastward. Thus, the response to El Niño is an anomalous center of convergence of mass in the upper troposphere across the Sahel (Figure 4b), which together with the mass divergence at the 850 mb level (Figure 4a) is indicative of

large-scale subsidence over the region. This is further confirmed through regression of the 500 mb level vertical wind anomalies on the same Niño 3.4 index (not shown).

4. Discussion and Conclusions

This study has shown that interannual-scale variability of Sahel rainfall is convincingly depicted in CAM5 when forced with historic SST observations, despite some limitations. The benefit of studying the model output is the increased ability to link rainfall mechanisms to SST change. A analysis of Sahel interannual precipitation variability and its links to global SST anomalies confirm the dominant role of ENSO, even though the model's forced signal is too weak compared to observations. We find consistency with prior studies that attribute high-frequency rainfall variability in the Sahel to conditions in the Pacific Ocean [*Giannini et al.*, 2003] through the atmosphere's dynamic circulation response to ENSO events [*Janicot et al.*, 1996; *Rowell*, 2001] utilizing a moisture budget approach. Net surface moisture in the Sahel is reduced during El Niño events primarily due to the reduction in moisture flux convergence by the mean flow and accomplished mostly through a reduction in atmospheric mass convergence. These are impacted substantially by the response of the large-scale atmospheric circulation to a heating anomaly over the Eastern Equatorial Pacific through a Gill-Matsuno mechanism. Anomalous upper tropospheric convergence and low-level mass divergence over North Africa are consistent with large-scale subsidence east of the area of Pacific heating, opposing conditions favorable for precipitation.

The present study builds upon prior work whose results document changes in WAM dynamics consistent with a dry Sahel [i.e., *Jenkins et al.*, 2005; *Sylla et al.*, 2013; *Diallo et al.*, 2013]. Similar changes are confirmed, providing further clarity through the moisture budget calculation as to how remotely forced (in this case by ENSO) dynamical changes translate to precipitation variability. Furthermore, our results agree qualitatively with previous studies that depict components of the moisture budget response to a "remote" source of heating, specifically for the case of Indian Ocean warming [*Hagos and Cook*, 2008]. The consistency between *Hagos and Cook* [2008] and the present study provides additional evidence that "remote" basins' influences on the Sahel come primarily through their effects on atmospheric circulation patterns and large-scale stability [*Giannini et al.*, 2008; *Giannini*, 2010; *Seth et al.*, 2011]. It has been noted that in order to fully disentangle climate projections for the Sahel, one needs to consider the competition between such remote influences and more local ones, specifically the role of the Atlantic Ocean in supplying enough moisture at low levels to overcompensate for increased convective thresholds [*Giannini et al.*, 2008, 2013]. The need for increased understanding of SST-forced variability as shown in this study thus cannot be overemphasized, particularly when considering the number of inhabitants who rely on monsoon rains for their livelihoods.

References

Alexander, M. A., I. Bladé, M. Newman, J. R. Lanzante, N.-C. Lau, and J. D. Scott (2002), The atmospheric bridge: The influence of ENSO teleconnections on air-sea interaction over the global oceans, *J. Clim.*, 15, 2205–2231, doi:10.1175/1520-0442(2002)015<2205:TABTIO>2.0.CO;2.

Bader, J., and M. Latif (2003), The impact of decadal-scale Indian Ocean sea surface temperature anomalies on Sahelian rainfall and the North Atlantic Oscillation, *Geophys. Res. Lett.*, 30(22), 2169, doi:10.1029/2003GL018426.

Bretherton, C. S., C. Smith, and J. M. Wallace (1992), An intercomparison of methods for finding coupled patterns in climate data, *J. Clim.*, 5, 541–560, doi:10.1175/1520-0442(1992)005<0541:AIOMFF>2.0.CO;2.

Diallo, I., M. B. Sylla, M. Camara, and A. T. Gaye (2013), Interannual variability of rainfall over the Sahel based on multiple regional climate models simulations, *Theor. Appl. Climatol.*, 113, 351–362, doi:10.1007/s00704-012-0791-y.

Folland, C. K., T. N. Palmer, and D. E. Parker (1986), Sahel rainfall and worldwide sea temperatures, 1901–85, *Nature*, 320, 602–607, doi:10.1038/320602a0.

Fontaine, B., P. Roucou, and S. Trzaska (2003), Atmospheric water cycle and moisture fluxes in the West African monsoon: Mean annual cycles and relationship using NCEP/NCAR reanalysis, *Geophys. Res. Lett.*, 30(3), 1117, doi:10.1029/2002GL015834.

Giannini, A. (2010), Mechanisms of climate change in the semiarid African Sahel: The local view, *J. Clim.*, 23, 743–756, doi:10.1175/2009JCLI3123.1.

Giannini, A., R. Saravanan, and P. Chang (2003), Oceanic forcing of Sahel rainfall on interannual to interdecadal time scales, *Science*, 302, 1027–1030, doi:10.1126/science.1089357.

Giannini, A., M. Biasutti, I. M. Held, and A. H. Sobel (2008), A global perspective on African climate, *Clim. Change*, 90, 359–383, doi:10.1007/s10584-008-9396-y.

Giannini, A., S. Salack, T. Lodoun, A. Ali, and O. Ndiaye (2013), A unifying view of climate change in the Sahel linking intra-seasonal, inter-annual and longer time scales, *Environ. Res. Lett.*, 8, doi:10.1088/1748-9326/8/2/024010.

Grist, J. P., and S. E. Nicholson (2001), A study of the dynamic factors influencing rainfall variability in the West African Sahel, *J. Clim.*, 14, 1337–1359, doi:10.1175/1520-0442(2001)014<1337:ASOTDF>2.0.CO;2.

Hagos, S. M., and K. H. Cook (2008), Ocean warming and late-twentieth-century Sahel drought and recovery, *J. Clim.*, 21, 3797–3814, doi:10.1175/2008JCLI2055.1.

Harris, I., P. D. Jones, T. J. Osborn, and D. H. Lister (2014), Updated high-resolution grids of monthly climatic observations—The CRU TS3.10 dataset, *Int. J. Climatol.*, *34*, 623–642, doi:10.1002/joc.3711.

Hoerling, M., J. Hurrell, J. Eischeid, and A. Phillips (2006), Detection and attribution of twentieth-century northern and southern African rainfall change, *J. Clim.*, *19*, 3989–4008, doi:10.1175/JCLI3842.1.

Janicot, S., V. Moron, and B. Fontaine (1996), Sahel droughts and ENSO dynamics, *Geophys. Res. Lett.*, *23*, 515–518, doi:10.1029/96GL00246.

Janicot, S., A. Harzallah, B. Fontaine, and V. Moron (1998), West-African monsoon dynamics and eastern equatorial Atlantic and Pacific SST anomalies (1970–1988), *J. Clim.*, *11*, 1874–1882.

Janicot, S., S. Trzaska, and I. Poccard (2001), Summer Sahel-ENSO teleconnection and decadal time scale SST variations, *Clim. Dyn.*, *18*, 303–320, doi:10.1007/s003820100172.

Jenkins, G. S., A. T. Gaye, and B. Sylla (2005), Late 20th century attribution of drying trends in the Sahel from the Regional Climate Model (RegCM3), *Geophys. Res. Lett.*, *32*, L22705, doi:10.1029/2005GL024225.

Kaplan, A., M. A. Cane, Y. Kushnir, A. C. Clement, M. B. Blumenthal, and B. Rajagopalan (1998), Analyses of global sea surface temperature 1856–1991, *J. Geophys. Res.*, *103*, 18,567–18,589, doi:10.1029/97JC01736.

Kucharski, F., A. Bracco, J. H. Yoo, A. M. Tompkins, L. Feudale, P. Ruti, and A. Dell'Aquila (2009), A Gill-Matsuno-type mechanism explains the tropical Altantic influence on African and Indian monsoon rainfall, *Q. J. R. Meteorol. Soc.*, *135*(640), 569–579, doi:10.1002/qj.406.

Lebel, T., A. Diedhiou, and H. Laurent (2003), Seasonal cycle and interannual variability of the Sahelian rainfall at hydrological scales, *J. Geophys. Res.*, *108*(D8), 8389, doi:10.1029/2001JD001580.

Li, L., W. Li, and A. P. Barros (2013), Atmospheric moisture budget and its regulation of the summer precipitation variability over the Southeastern United States, *Clim. Dyn.*, *41*, 613–631, doi:10.1007/s00382-013-1697-9.

Lu, J. (2009), The dynamics of the Indian Ocean sea surface temperature forcing of Sahel drought, *Clim. Dyn.*, *33*, 445–460, doi:10.1007/s00382-009-0596-6.

Neale, R. B., et al. (2012), Description of the NCAR Community Atmosphere Model (CAM 5.0), *NCAR Tech. Note TN-486*, 289 pp.

Nicholson, S. E. (2000), The nature of rainfall variability over Africa on time scales of decades to millennia, *Global Planet. Change*, *26*, 137–158, doi:10.1016/S0921-8181(00)00040-0.

Nicholson, S. E., and P. J. Webster (2007), A physical basis for the interannual variability of rainfall in the Sahel, *Q. J. R. Meteorol. Soc.*, *133*(629), 2065–2084, doi:10.1002/qj.104.

Palmer, T. N. (1986), Influence of the Atlantic, Pacific, and Indian Oceans on Sahel rainfall, *Nature*, *322*, 251–253, doi:10.1038/322251a0.

Pomposi, C., Y. Kushnir, and A. Giannini (2014), Moisture budget analysis of SSTdriven decadal Sahel precipitation variability in the twentieth century, *Clim. Dyn.*, *44*, 3303–3321, doi:10.1007/s00382-014-2382-3.

Rayner, N. A., D. E. Parker, E. B. Horton, C. K. Folland, L. V. Alexander, D. P. Rowell, E. C. Kent, and A. Kaplan (2003), Global analyses of sea surface temperature, sea ice, and night marine air temperature since the late nineteenth century, *J. Geophys. Res.*, *108*(D14), 4407, doi:10.1029/2002JD002670.

Rowell, D. P. (2001), Teleconnections between the tropical Pacific and the Sahel, *Q. J. R. Meteorol. Soc.*, *127*(575), 1683–1706, doi:10.1002/qj.49712757512.

Rowell, D. P., C. K. Folland, K. Maskell, and M. N. Ward (1995), Variability of summer rainfall over tropical north Africa (1906–92): Observations and Modelling, *Q. J. R. Meteorol. Soc.*, *121*(523), 669–704, doi:10.1002/qj.49712152311.

Seager, R., and N. Henderson (2013), Diagnostic computation of moisture budgets in the ERA-Interim reanalysis with reference to analysis of CMIP-archived atmospheric model data, *J. Clim.*, *26*, 7876–7901, doi:10.1175/JCLI-D-13-00018.1.

Seager, R., N. Naik, and G. A. Vecchi (2010), Thermodynamic and dynamic mechanisms for large-scale changes in the hydrological cycle in response to global warming, *J. Clim.*, *23*, 4651–4668, doi:10.1175/2010JCLI3655.1.

Seth, A., S. A. Rauscher, M. Rojas, A. Giannini, and S. J. Camargo (2011), Enhanced spring convective barrier for monsoons in a warmer world?, *Clim. Change*, *104*, 403–414, doi:10.1007/s10584-010-9973-8.

Sylla M. B., I. Diallo, and J. S. Pal (2013), West African monsoon in state-of-the-science regional climate models, in *Climate Variability—Regional and Thematic Patterns*, edited by A. Tarhule, InTech, Rijeka, Croatia, doi:10.5772/55140.

Thorncroft, C., H. Nguyen, C. Zhang, and P. Peyrillé (2011), Annual cycle of the West African monsoon: Regional circulations and associated water vapor transport, *Q. J. R. Meteorol. Soc.*, *137*(654), 129–147, doi:10.1002/qj.728.

Ward, N. M. (1998), Diagnosis and short-lead time prediction of summer rainfall in tropical North Africa at interannual and multidecadal timescales, *J. Clim.*, *11*, 3167–3191, doi:10.1175/1520-0442(1998)011<3167:DASLTP>2.0.CO;2.